

# Helicity and topology of a small region of quantum vorticity

M. Mesgarnezhad<sup>1</sup>, R.G. Cooper<sup>1</sup>, A.W. Baggaley<sup>1</sup> and C.F. Barenghi<sup>1</sup>

<sup>1</sup> *School of Mathematics and Statistics and Joint Quantum Centre Durham-Newcastle,  
Newcastle University, Newcastle upon Tyne NE1 7RU, UK\**

## Abstract

We numerically study the evolution of a small turbulent region of quantised vorticity in superfluid helium, a regime which can be realised in the laboratory. We show that the turbulence achieves a fluctuating steady-state in terms of dynamics (energy), geometry (length, writhing) and topology (linking). We show that, at any instant, the turbulence consists of many unknots and few large loops of great geometrical and topological complexity.

arXiv:1610.10024v2 [cond-mat.other] 28 Mar 2017

---

\* m.mesgarnezhad1@newcastle.ac.uk

*Keywords:* Hydrodynamic aspects of superfluidity, Vortices and turbulence, Quantum vorticity

## I. INTRODUCTION

Tangled filamentary structures occur in many physical systems, from ropes to optics [1] to DNA [2]. Concentrated field lines in fluids [3] and plasmas [4] (e.g. vortex lines and magnetic field lines) are another important example. Such lines undergo reconnection events, which are associated with energy losses. In the limit of no dissipation, the governing equations of motion (the Euler equation and the magnetic induction equation in the frozen field approximation respectively) preserve the topology of the lines. In this limit, helicity and magnetic helicity are conserved quantities. Recent work suggests that, in the case of small dissipation, helicity is partially preserved [5]. The aim of this work is to explore this partial preservation of helicity in a context where vortex lines are not mathematical abstractions but have a real physical meaning: this is the context of quantum fluids, notably superfluid liquid helium ( $^4\text{He}$  and  $^3\text{He}$ ) and atomic Bose-Einstein condensates. The numerical experiment which we describe explores the relation between geometry, dynamics and topology of a small region of turbulence in superfluid helium.

## II. QUANTUM VORTICITY

Quantum fluids are characterised by zero viscosity and the quantisation of the circulation. The first property makes superfluids similar to inviscid Euler fluids of traditional textbooks. The second property arises from the existence of a complex macroscopic wavefunction  $\Psi(\mathbf{x}, t) = \sqrt{n(\mathbf{x}, t)}e^{i\phi(\mathbf{x}, t)}$  where  $\mathbf{x}$  is the position,  $t$  is the time,  $n(\mathbf{x}, t)$  is the number density; according to the Madelung transformation [6], the superfluid velocity is proportional to the gradient of the phase:

$$\mathbf{v}(\mathbf{x}, t) = \frac{\hbar}{m} \nabla \phi, \quad (1)$$

where  $m$  is the mass of the relevant boson ( $m = 6.6 \times 10^{-27}$  kg for  $^4\text{He}$ ),  $\hbar = h/(2\pi)$  and  $h = 6.6 \times 10^{-34}$  J s is Planck's constant. The single-valuedness of  $\Psi$  implies that the circulation of the superfluid velocity field around a closed path  $C$  is either zero or a multiple of the quantum of circulation  $\kappa = h/m$ :

$$\oint_C \mathbf{v} \cdot d\mathbf{r} = n\kappa, \quad (2)$$

( $n = 0, \pm 1, \pm 2, \dots$ ). Nonzero circulation occurs when the path  $C$  encloses a vortex line; in this case  $\Psi = 0$  on the axis of the vortex line. Since multi-charged ( $|n| > 1$ ) vortices are unstable, we are concerned only with the case  $n = \pm 1$ . Around the axis of the vortex line there is a thin tubular region of depleted density of radius  $a_0 \approx 10^{-10}$  m in  ${}^4\text{He}$ ; in this region, the density  $n(\mathbf{x}, t)$  drops from its bulk value at infinity to zero on the vortex axis. In summary, a vortex line is a hole with superfluid circulation around it. As in classical fluid dynamics, quantum vortex lines are either closed loops or terminate at boundaries.

An isolated vortex is a stable topological defect which does not decay, unlike vortices in ordinary viscous fluids. Numerical simulations of the governing Gross-Pitaevskii equation for  $\Psi$  show that vortex lines reconnect when they come close to each other [8–10], as observed in experiments in superfluid helium [11] and, more recently, in atomic condensates [12]. In this process, some of the kinetic energy of the vortices is turned into density waves [9, 13]. Evidently, vortex reconnections are of particular important for the dynamics of turbulence in superfluid helium [14] and in atomic Bose-Einstein condensates [15].

In typical experiments the average distance between vortices,  $\ell \approx 10^{-4}$  to  $10^{-2}$  m, is many orders of magnitude larger than the vortex core radius  $a_0$ . It is therefore appropriate to model quantum vortices as (closed) space curves  $\mathbf{s}(\xi, t)$  (where  $\xi$  is arc-length) of infinitesimal thickness. In a pure superfluid (e.g. liquid helium at temperatures below 1 K) thermal excitations are particularly negligible, and the vortex moves according to [16]

$$\frac{d\mathbf{s}}{dt} = \mathbf{v}_{self}(\mathbf{s}), \quad (3)$$

where the self-induced velocity  $\mathbf{v}_{self}$  is given by the classical Biot-Savart law:

$$\mathbf{v}_{self}(\mathbf{s}) = -\frac{\kappa}{4\pi} \oint_{\mathcal{L}} \frac{(\mathbf{s} - \mathbf{r}) \times d\mathbf{r}}{|\mathbf{s} - \mathbf{r}|^3}. \quad (4)$$

(the line integral extending over the entire vortex configuration  $\mathcal{L}$ ). Numerical simulations of quantum vortex lines are based on Lagrangian discretisation of the lines [7]. The number of discretisation points along a line varies, as more/less points are required in regions of high/low curvature. The Biot-Savart integral is de-singularised in a standard way [7] (based on the distance  $a_0$ ), and an algorithmic reconnection procedure is implemented [17]. The numerical method is standard and has been published in the literature [18, 19].

In this work, we are concerned with (experimentally easily accessible) high temperatures

( $T > 1$  K). In this regime, the thermal excitations form a viscous fluid (called the normal fluid) of velocity field  $\mathbf{v}_n$  which exchanges energy with the vortex line via a mutual friction force [20]. Eq. (3) requires modifications, and becomes [7]

$$\frac{d\mathbf{s}}{dt} = \mathbf{v}_{self} + \alpha \mathbf{s}' \times (\mathbf{v}_n - \mathbf{v}_{self}) - \alpha' \mathbf{s}' \times [\mathbf{s}' \times (\mathbf{v}_n - \mathbf{v}_{self})]. \quad (5)$$

Here  $\alpha$  and  $\alpha'$  are small temperature-dependent friction coefficients arising from the interaction of the vortex lines with the thermal excitations which make up the normal fluid (if  $T \rightarrow 0$  then  $\alpha \rightarrow 0$  and  $\alpha' \rightarrow 0$ , recovering Eq. (3)). It must be stressed that the friction force is a two-way route to exchange energy between the normal fluid and the superfluid vortex lines. If a section of a vortex line is exposed to normal flow  $\mathbf{v}_n$  locally aligned in the same direction of the superfluid vorticity and with intensity larger than a certain critical value, infinitesimal perturbations on that section of the vortex line will grow in length in the form of Kelvin waves (helical displacements of the vortex axis away from its initial position); this effect is called the Glaberson-Donnelly instability [21]. Vice-versa, if  $\mathbf{v}_n$  is perpendicular to the vortex line or if  $\mathbf{v}_n = 0$ , the friction will dissipate the Kelvin waves. Similarly, if  $\mathbf{v}_n$  blows along the direction of propagation of a superfluid vortex ring, the ring will increase its radius; vice-versa, if  $\mathbf{v}_n$  blows in the opposite direction or if  $\mathbf{v}_n = 0$ , the ring will shrink and vanish.

### III. TURBULENT QUANTUM VORTICITY

Our aim is to numerically simulate a state of turbulence of vortex lines which has two properties: (i) it is in a statistical steady-state (independent of the arbitrary initial condition, unlike previous work [22] which was concerned with comparing energy and complexity during an initial transient), and (ii) is away from (hard or periodic) boundaries (so that vortex lines are closed loops and the definition of linking is simple and unambiguous).

It is not trivial to satisfy (i) and (ii) at the same time. Most experiments and numerical simulations of quantum turbulence have been performed within hard or periodic boundaries. In these studies, after an initial transient, a steady-state regime is achieved and the vortex lines fill the entire domain, which means that some vortex lines are not closed loops but terminate at the boundaries. Because of the Lagrangian discretisation, calculations can also be performed in open, infinite domains, but in this case the vortex length will grow without

limit.

The calculations which we present here model experiments [23, 24] in which ultra-sound waves were focused at the centre of the experimental cell creating vortex lines away from boundaries. In this experiments, vortex lines which left the central region decayed due to friction with the normal fluid which was stationary far from the central region. To model this experimental configuration we impose a time-dependent, space dependent velocity field  $\mathbf{v}_n$  in the form of random waves [25] near the centre of the computational domain; away from the centre, we impose that the normal fluid velocity decays exponentially - see Fig. (1). In the central region we place typically 40 vortex rings (planar unknots) as seeding initial condition at  $t = 0$ . The images which we present mainly refer to a numerical simulation in which the initial rings have the same radius but random orientation, and their centres are shifted according to a normal distribution, but it is important to note that we have performed simulations starting from different initial conditions (e.g. rings of random positions and sizes) and longer times in statistical steady-state regime, and the results appear to be independent of the precise initial vortex configuration. All numerical simulations are performed at a temperature  $T = 1.9$  K (corresponding to  $\alpha = 0.206$  and  $\alpha' = 8.34 \times 10^{-3}$ ) which is typical of experiments.

During the evolution, we observe that the vortex length rapidly increases in the central region due to the Donnelly-Glaberson instability, resulting in Kelvin waves and vortex reconnections (which continuously change the number of vortex loops); a turbulent tangle of vortex lines quickly grows, as shown in Fig. (2).

We have not measured directly the distribution of angles  $\theta$  between reconnecting vortex lines during our numerical simulations, but recall the results of a previous study[26] which determined  $\theta$  for two different fully-developed turbulent regimes. In the first regime, the turbulence exhibited a classical Kolmogorov cascade (energy spectrum concentrated at the largest length scales followed by  $k^{-5/3}$  scaling at larger wavenumbers  $k$ ), and the distribution of the reconnecting angles  $\theta$  peaked at small angles ( $\theta \approx \pi/8$  in Fig. 9 of cited reference). Indeed, the vortex tangle visibly contained metastable bundles of parallel vortices, making parallel reconnections relatively more frequent. In the second regime, the turbulence did not exhibit any sign of a classical cascade (energy spectrum concentrated at the mesoscales and  $k^{-1}$  scaling at larger  $k$ ), the distribution of reconnection angles peaked at larger angles closer to 180 degrees ( $\theta \approx 7\pi/8$  in Fig. 9 of cited reference). Indeed, the vortex tangle

lacked bundles and looked more random, making antiparallel reconnections relatively more frequent. We believe that the relatively small vortex configurations which we study here are more similar to the second regime: they are visibly more random-looking and lack the large separation of length scales between the average intervortex spacing and the system's size for the classical Kolmogorov spectrum to develop. We expect therefore that antiparallel reconnections are relatively more frequent.

After a quick initial transient, a balance is reached between vortex generation and vortex decay in the central region, and the vortex length saturates. Vortex loops which drift too far away from the central region decay due to friction with the stationary normal fluid in the outer region; this effect helps create the desired saturated, localised region of quantum turbulence. characterised by fluctuations of the vortex length  $\Lambda$  about an average value, as shown in Fig. (3). The small loops which drift away and escape from the central region are either rings or slightly deformed rings (that is to say unknots). Larger more knotted structures are slower and cannot escape easily from the central region (if they did, friction with the normal fluid would lead them to shrink, thus eventually reconnect, turning them into unknots).

In Fig. (2), note that the tangle does not necessarily remain isotropic during the evolution: given the random nature of the driving  $\mathbf{v}_n$  and the exponential growth of the Donnelly-Glaberson instability, a particular realisation of the synthetic turbulence may generate a vortex configuration which moves off-centre or does not extend by the same amount in all directions.

#### IV. GEOMETRY AND TOPOLOGY OF THE TURBULENCE

In this section we analyse the dynamical, geometrical and topological properties of the steady-state regime of quantum turbulence which we have achieved. We have checked that not only the length, but also the kinetic energy  $E$  of the vortex lines saturates to an average value, see Fig. (4). The energy is evaluated from [16]

$$E = \int_V \mathbf{v} \cdot \mathbf{r} \times \boldsymbol{\omega} dV, \quad (6)$$

(where  $V$  is volume). In our case, assuming that  $\mathbf{v} \rightarrow 0$  at infinity, since vorticity is concentrated along filaments, Eq. (6) reduces to

$$E = \kappa \oint_{\mathcal{L}} \mathbf{v} \cdot \mathbf{r} \times d\mathbf{s}', \quad (7)$$

where the line integral extends over the entire vortex tangle  $\mathcal{L}$ . A quantity which is often reported in the literature as a measure of the turbulent intensity is the vortex line density (length of vortex line per unit volume), defined as  $L = \Lambda/V$ . Without boundaries, the volume which contains the lines is not a well-defined quantity; we estimate it as the sphere which contains 95% of the vortex lines. In the simulation shown in Fig. (3), we obtain  $L \approx 2500 \text{ cm}^{-2}$

Further analysis is performed using the concept of *crossing numbers*. At a given instant, the turbulent vortex tangle consists of a number of vortex loops:  $\mathcal{L} = \cup_j \mathcal{L}_j$ . We project the tangle  $\mathcal{L}$  onto a given 2D plane. The projected tangle is a self-intersecting curve: the points of intersection correspond to apparent crossings of  $\mathcal{L}$  as seen from the line of sight of the projection. Since each loop is oriented (by the sense of rotation of the superfluid velocity), we can assign values  $\epsilon_k = \pm 1$  to each point of intersection  $k$  according to standard convention, see Fig. (5). The total number of crossings,  $k$ , is plotted vs time in Fig. (6); this is the simplest measure of the complexity of the tangle. We can also readily define the *writhing number* of the entire tangle as

$$W = \left\langle \sum_{k \in \mathcal{L}} \epsilon_k \right\rangle, \quad (8)$$

where the symbol  $\langle \dots \rangle$  denotes the average over a number of projections to make the result independent of a particular projection [22]. Ideally, the writhing number should be estimated by integrating over all solid angles; in practice, this would be computationally expensive. Numerical experiments [22] suggest it suffices to average over a small number of projections. The results which we report are calculated simply by projecting over the three Cartesian planes. We find - see Fig. (7) - that the writhing number of the tangle achieves a statistically steady-state too.

Other geometrical and topological properties of individual vortex loops  $\mathcal{L}_j$  or of the entire tangle  $\mathcal{L}$  can be evaluated by suitably conditioning Eq. (8). For example, the writhing number  $W_j$  of an individual loop  $\mathcal{L}_j$  is obtained by summing the crossing numbers restricted to vortex strands which belong to that particular loop:



$$Wr_j = \left\langle \sum_{k \in \mathcal{L}_j} \epsilon_k \right\rangle. \quad (9)$$

Another quantity of interest is the *linking number*  $Lk_{i,j}$  between loops  $\mathcal{L}_i$  and  $\mathcal{L}_j$ , which is defined as

$$Lk_{i,j} = \frac{1}{2} \sum_{k \in \mathcal{L}_i \cap \mathcal{L}_j} \epsilon_k. \quad (10)$$

This quantity, computed from a single arbitrary projection, is the same for any projection, as it can be easily verified [27]. A measure of the topological complexity of the turbulence is the *total linkage*  $Lk$  of the tangle, defined as

$$Lk = \sum_i \sum_{j \neq i} |Lk_{i,j}|. \quad (11)$$

The physical importance of the linkage is that only vortex reconnections can undo the linking between two loops and each reconnection has an energy cost (in terms of sound waves emitted). The total linkage vs time is shown in Fig. (8). It is apparent that the fluctuations of the linkage are relatively large, as few reconnections make a relatively large change for a small vortex configuration like ours, but the turbulence settles to an average value of linkage, which is  $\bar{Lk} = 54.07$  in Fig. (8). The spontaneous formation of links has also been observed in a numerical simulation of decaying turbulence using the Gross-Pitaevskii equation [28].

Now we turn the attention to the *helicity*. In a classical fluid, the helicity is defined as [29]

$$H = \int_V \mathbf{v} \cdot \boldsymbol{\omega} dV, \quad (12)$$

where  $\boldsymbol{\omega}$  is the vorticity. What should be the correct definition of helicity in a quantum fluid is a hot topic in the current literature [30–32]. The difficulty is that, on one hand, we would like a definition of helicity which is consistent with the classical definition of helicity, and, on the other hand, in a quantum fluid vorticity  $\boldsymbol{\omega}$  is zero everywhere with the exception of the axes of vortex lines; more precisely,  $\boldsymbol{\omega}$  is a delta function on the vortex axis, which unfortunately is also the location where the velocity is undefined. It is worth remarking that in a classical fluid one thinks of the vortex core as a small bundle of mathematical vortex

lines; this allows an interpretation of helicity which contains internal twist. In a quantum fluid, however, there is *only one vortex line* (on the axis of the vortex - everywhere else the flow is potential). For the sake of simplicity, we follow Scheeler et al [33] and interpret  $H$  as *centreline helicity* defined as

$$H = \kappa^2 \left( 2 \sum_i \sum_{j \neq i} Lk_{i,j} + \sum_i Wr_i \right). \quad (13)$$

An important physical property of the centreline helicity is that it is invariant under anti-parallel reconnections characteristic of fluid flows [34]. Fig. (9) shows that the centreline helicity remains approximately constant during the time evolution. After the initial transient, the average value is  $\bar{H} \approx -96.39\kappa^2$ .

We also characterise the complexity of the turbulence by computing the relative distribution of vortex loops with a given value of writhe. The relative writhe distribution suggests that although most loops have a small value of  $|Wr_j|$ , at any instant there is a consistent number of loops with large value of writhe (see Fig. 10) in the approximate range  $50 < |Wr_j| < 300$ . Closer investigation confirms that these complex loops with more coils and twists than the average loop keep forming, decaying and reforming. Examples of vortex loops with small and large values of  $|Wr_j|$  are shown in Fig. (11).

The geometrical complexity described by the writhe spectrum seems associated with a similar topological complexity. A simple way to quantify the topology of a vortex loop is to determine the order  $A$  of its Alexander polynomial [35]. The Alexander polynomial  $\Delta(\tau)$  is a topological invariant which can be easily computed by labelling segments of a loop between under-crossings when projected into a plane, followed by assigning coefficients to the relevant entries of a matrix for each segment, and then finding the determinant of the matrix with any single row and column removed [36]. Given the vortex configuration at any time  $t$ , we compute the Alexander polynomial of each vortex loop and find its order  $A$ . For example the Alexander polynomial of the trivial unknot is  $\Delta(\tau) = 1$  hence its order is  $A = 0$ . The simplest knot is the trefoil ( $3_1$ ) knot, which has Alexander polynomial  $\Delta(\tau) = 1 - \tau + \tau^2$ , hence its order is  $A = 2$ . Any vortex loop which has an Alexander polynomial of order  $A > 0$  is knotted, however the converse is not necessarily true: a long-standing problem of knot theory is the lack of a unique method of distinguishing knots from each other. In particular, the Alexander polynomial is not unique to a particular knot type. For example

there exist knots which have the same Alexander polynomial as the unknot [37], so the fact that a vortex loop has an Alexander polynomial of order  $A = 0$  does not necessarily imply that it is an unknot. Nevertheless, the order of the Alexander polynomial of a loop is a more instructive measure of the loop's topology than its writhe.

The distribution of values of  $A$  is similar to the distribution of values of  $|Wr_j|$ : we find that, at any instant, most vortex loops are unknots, but, there are always some loops with a high degree of topological complexity in the approximate range  $25 < A < 125$ . Fig. 12 shows the distribution of values of  $A$  for the three most complex knots in a given vortex configuration (that is, at each instant  $t$  for a sample of values of  $t$ ): the figure confirms the robustness of the finding - in any vortex configuration there is always a small but consistent number of loops with nontrivial topology. Some examples of vortex loops with intermediate and large values of  $A$  which we observed in our numerical simulations are shown in Fig. (13).

Finally, Fig. (14) shows the relationship between the length of vortex loops,  $\Lambda_j$ , and the order of their Alexander polynomials,  $A$ . It is apparent that complex knots tend to be long knots. The inset plots the data on linear-log scales and suggests that  $A$  increases roughly exponentially with  $\Lambda_j$ . It is interesting to remark that the probability that a DNA molecule (modelled as a random polygon) is unknotted decreases exponentially with length toward zero[38].

## V. CONCLUSION

In conclusion, we have simultaneously related geometry, dynamics and topology of a small statistically-steady turbulent region of quantum vorticity away from boundaries; we have chosen such a regime because it simplifies the calculation of topological properties and can be generated in the laboratory. We have shown that centreline helicity is preserved in a statistical steady-state regime like energy, length, writhing and linking. By examining the writhe and the order of the Alexander polynomial of vortex loops, we have found that most of the loops are topologically trivial (unknots), but there are always some vortex loops of great geometrical and topological complexity.

Further work will study how the complexity increases with the intensity of the turbulence and look for scaling laws. Another line of further work would be to replace the driving random waves with a Beltrami flow, seeking to induce more helicity in the turbulence.

The saturation process would proceed as described here, but we would have less relative fluctuations of helicity.

## ACKNOWLEDGMENTS

We thank Prof DW Sumners and Dr A Duncan for discussions, and EPSRC (grant EP/I019413/1) for financial support.

## REFERENCES

---

- [1] Padgett MJ, O'Holleran K, King RP and Dennis MR 2011 *Contemporary Physics* **52** 265
- [2] Vologodskii AV, Crisona NJ, Laurie B, Pieranski P, Katritch V, Dubochet J, Stasiak A 1998 *J Mol. Bio.* **278** 1
- [3] Kida S and Takaoka M 1994 *Ann. Rev. Fluid Mech.* **26** 169
- [4] Priest E and Forbes T 2000 *Magnetic Reconnections* (Cambridge: Cambridge University Press)
- [5] Kleckner D, Kauffman LH and Irvine TM 2015 *Nature Phys.* **9** 253
- [6] Barenghi CF and Parker NG 2016 *A Primer on Quantum Fluids* (Springer)
- [7] Schwarz KW 1988 *Phys. Rev. B* **38** 2398
- [8] Koplik J and Levine H 1993 *Phys. Rev. Letters* **71** 1375
- [9] Zuccher S, Caliari M, Baggaley AW and Barenghi CF 2012 *Phys. Fluids* **24** 125108
- [10] Allen AJ, Zuccher S, Caliari M, Proukakis NP, Parker NG and Barenghi CF 2014 *Phys. Rev. A* **90** 013601
- [11] Bewley GP, Paoletti MS, Sreenivasan KR and Lathrop DP 2008, *Proc Natl Acad Sci USA* **105** 13707
- [12] Serafini S, Barbiero M, Debortoli M, Donadello S, Larcher F, Dalfovo F, Lamporesi G and Ferrari G 2015, *Phys. Rev. Lett.* **115** 170402
- [13] Leadbeater M, Winiecki T, Samuels DC, Barenghi CF and Adams CS 2001 *Phys Rev Lett* **86** 1410

- [14] Barenghi CF, Skrbek L and Sreenivasan KR 2014 *Proc Nat Acad Sciences USA* **111** (Suppl. 1) 4647
- [15] Tsatsos MC, Tavares PES, Cidrim A, Fritsch AR, Caracanhas MA, dos Santos EA, Barenghi CF and Bagnato VS 2016 *Phys. Reports* **622** 1.
- [16] Saffman PG 1992 *Vortex Dynamics* (Cambridge: Cambridge University Press)
- [17] Baggaley AW 2012 *J Low Temp Phys* **68** 18
- [18] Adachi H, Fujjyama S and TsubotaM 2010 *Phys. Rev. B* **81** 104511
- [19] Baggaley AW and Barenghi CF 2012 *J Low Temp Phys* **166** 3
- [20] Barenghi CF, Donnelly RJ and Vinen WF 1983 *J Low Temp Phys* **52** 189
- [21] Ostermeier RM and Glaberson 1975 *J Low Temp Phys* **21** 191
- [22] Barenghi CF, Ricca RL and Samuels CS 2001 *Physica D* **157** 197
- [23] Schwarz KW and Smith CW 1981 *Phys Lett* **82A** 251
- [24] Milliken FP. Schwarz KW and Smith CW 1982 *Phys Rev Lett* **48** 1204
- [25] Baggaley AW and Barenghi CF 2011 *Phys Rev* **E84** 067301
- [26] Baggaley AW, Sherwin LK, Barenghi CFB and Sergeev YA 2012, *Phys Rev B* **86**, 104501
- [27] Kauffman LH 1987 *On Knots* (Princeton University Press, Princeton)
- [28] Villois A, Proment D and Krstulovic G 2016, *Phys. Rev. E* **93** 061103(R)
- [29] Moffatt HK 1969 *J Fluid Mech* **35** 117
- [30] Clark di Leoni P, Mininni PD and Brachet ME 2016 *Phys Rev A* **94** 043605
- [31] Zuccher S and Ricca RL 2015 *Phys. Rev. E* **92** 061001(R)
- [32] Hänninen R, Hietala N and Salman H 2016 *Sci Reports* **6** 37571
- [33] Scheeler MW, Kleckner D, Proment D, Kindlmann GL and Irvine WTM 2014 *Proc Natl Acad Sci USA* **111** 15350
- [34] Laing CE, Ricca RL and Sumners De Witt L 2015 *Sci Reports* **5** 9224
- [35] Alexander JW 1928 *Trans. Amer. Math. Soc* **30** 275
- [36] Livingstone L 1993 *Knot Theory* (Cambridge: Cambridge University Press)
- [37] Des Cloizeaux J and Mehta ML 1979 *J de Physique* **40** 665
- [38] Arsuaga J, Vazquez M, Trigueros S, Sumners De Witt L and Roca J 2002 *Proc Nat Acad Sci USA* **99** 5373

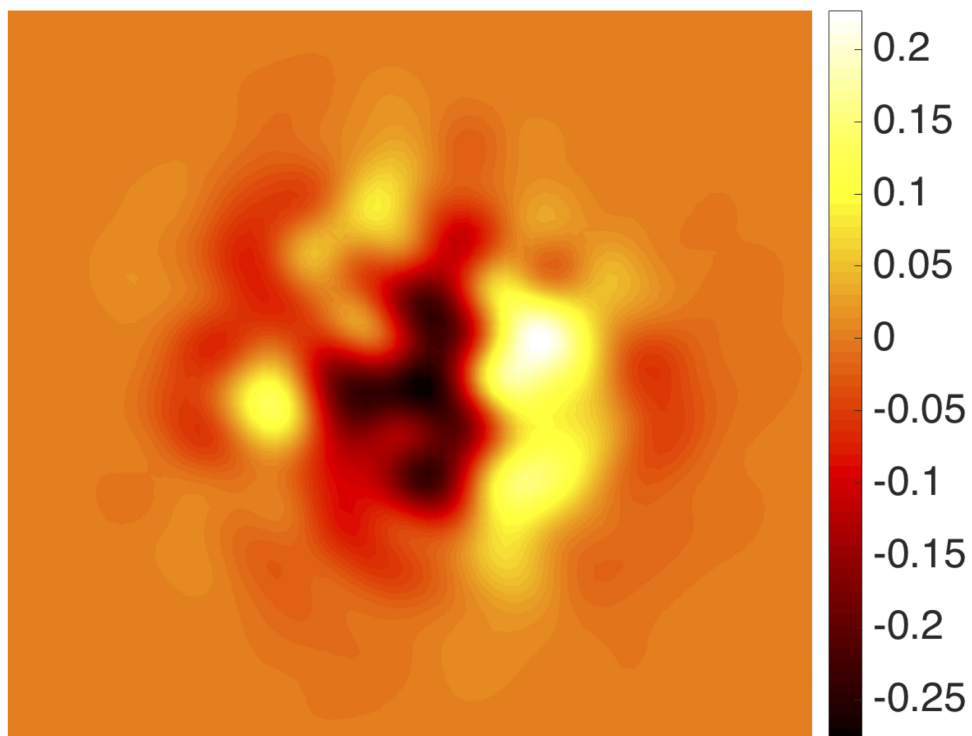


FIG. 1. Intensity of the normal fluid velocity  $\mathbf{v}_n$  at an arbitrary time plotted on the  $z = 0$  plane.

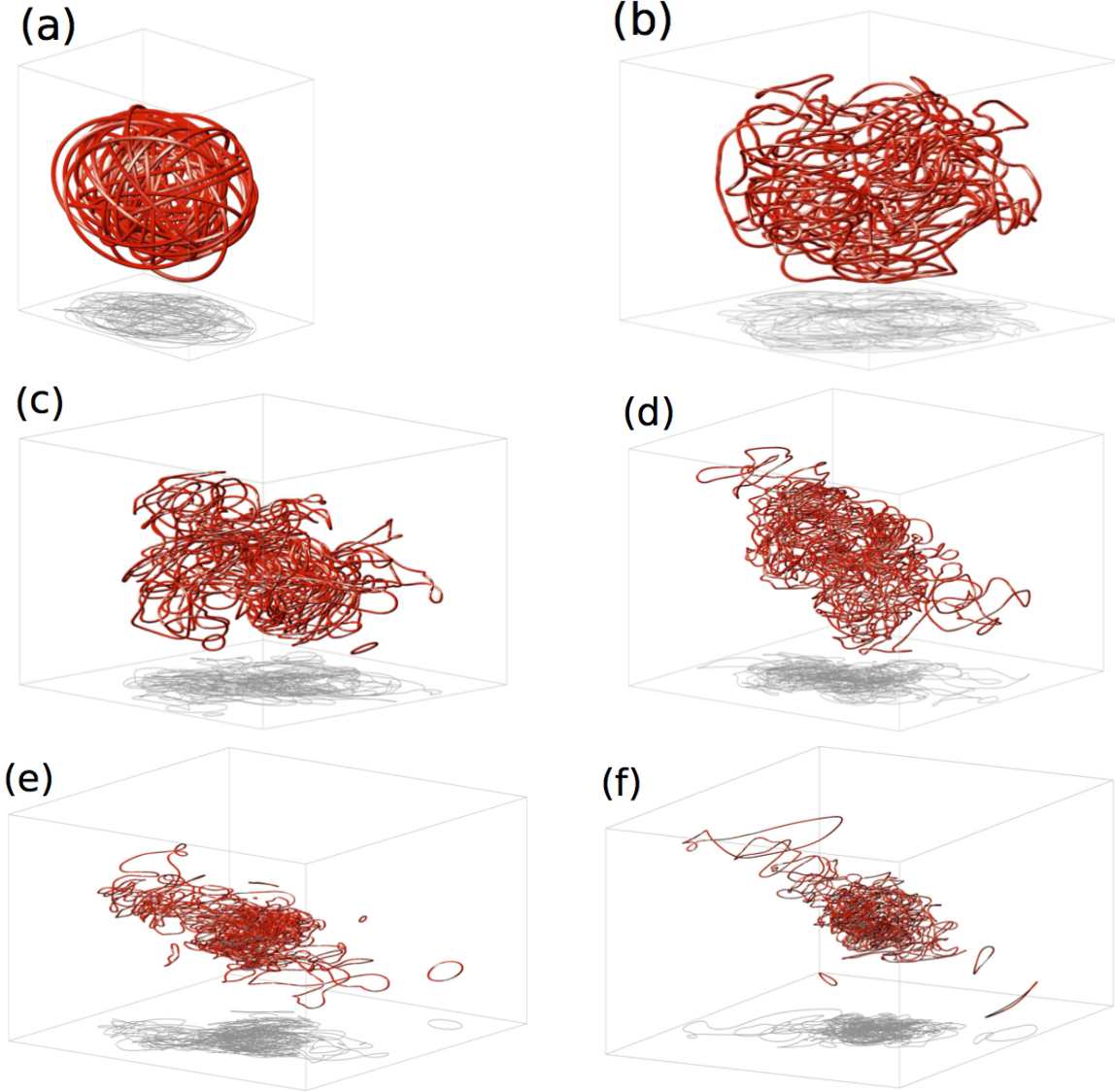


FIG. 2. Typical time evolution of the vortex tangle. The vortex lines are the red curves enclosed in a box with shadows for visualisation purposes only. The figure shows the vortex tangle at

- (a):  $t=0.00\text{s}$  in the region  $-0.02 \leq x \leq 0.02$ ,  $-0.02 \leq y \leq 0.02$ ,  $-0.03 \leq z \leq 0.02$
- (b):  $t=0.04\text{s}$  in the region  $-0.08 \leq x \leq 0.07$ ,  $-0.08 \leq y \leq 0.06$ ,  $-0.09 \leq z \leq 0.08$
- (c):  $t=0.20\text{s}$  in the region  $-0.11 \leq x \leq 0.10$ ,  $-0.11 \leq y \leq 0.10$ ,  $-0.12 \leq z \leq 0.13$
- (d):  $t=0.80\text{s}$  in the region  $-0.13 \leq x \leq 0.16$ ,  $-0.14 \leq y \leq 0.15$ ,  $-0.19 \leq z \leq 0.16$
- (e):  $t=1.60\text{s}$  in the region  $-0.16 \leq x \leq 0.18$ ,  $-0.15 \leq y \leq 0.20$ ,  $-0.29 \leq z \leq 0.29$
- (f):  $t=4.00\text{s}$  in the region  $-0.25 \leq x \leq 0.23$ ,  $-0.25 \leq y \leq 0.22$ ,  $-0.30 \leq z \leq 0.27$ .

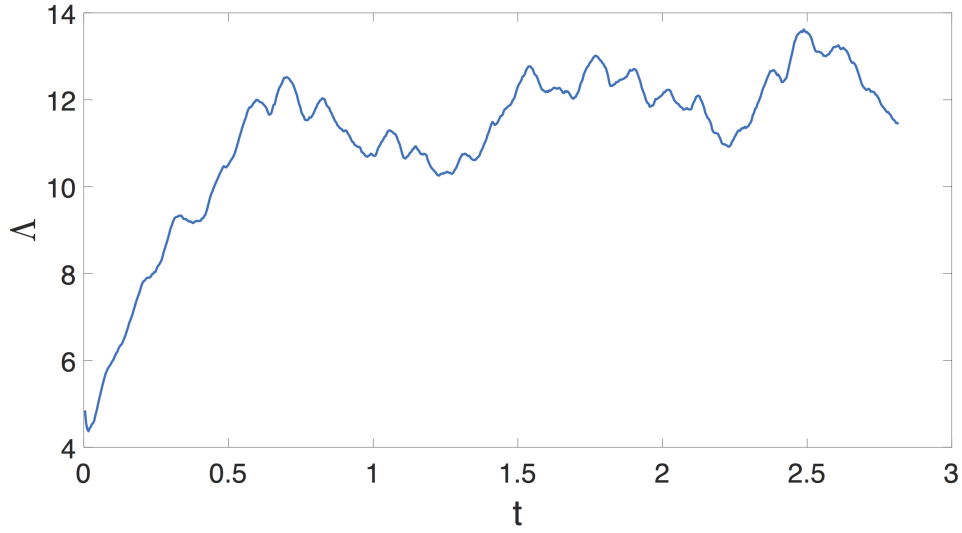


FIG. 3. Length  $\Lambda$  of the vortex configuration (in cm) vs time  $t$  (in s). At  $t = 0$ , the initial length of this realisation is  $\Lambda(0) = 4.0\text{cm}$  and the average length for  $t > 0.6$  is  $\bar{\Lambda} = 11.77\text{cm}$ .

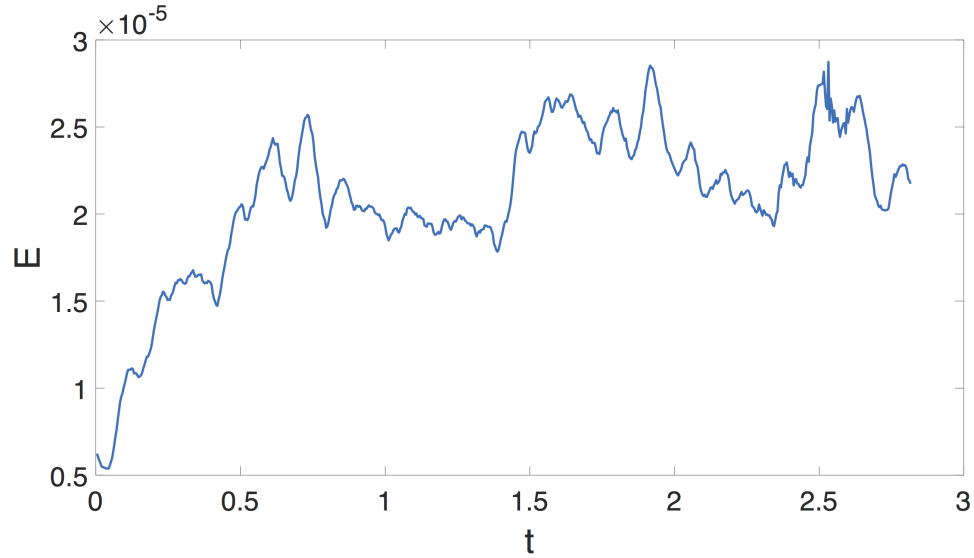


FIG. 4. Kinetic energy  $E$  of the vortex configuration (arbitrary units) vs time  $t$  (in s) corresponding to Fig. (2). The average energy for  $t > 0.6$  is  $\bar{E} = 2.20 \times 10^{-5}$ .



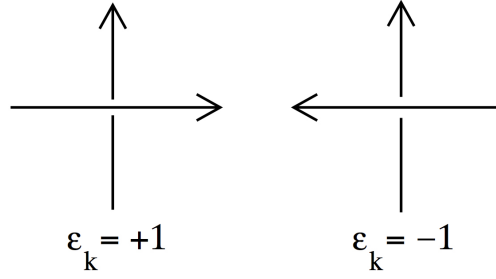


FIG. 5. Each point of intersection  $k$  of the projected tangle is assigned a crossing number  $\epsilon_k = \pm 1$  depending on the relative orientation of the vortex lines as schematically shown here.

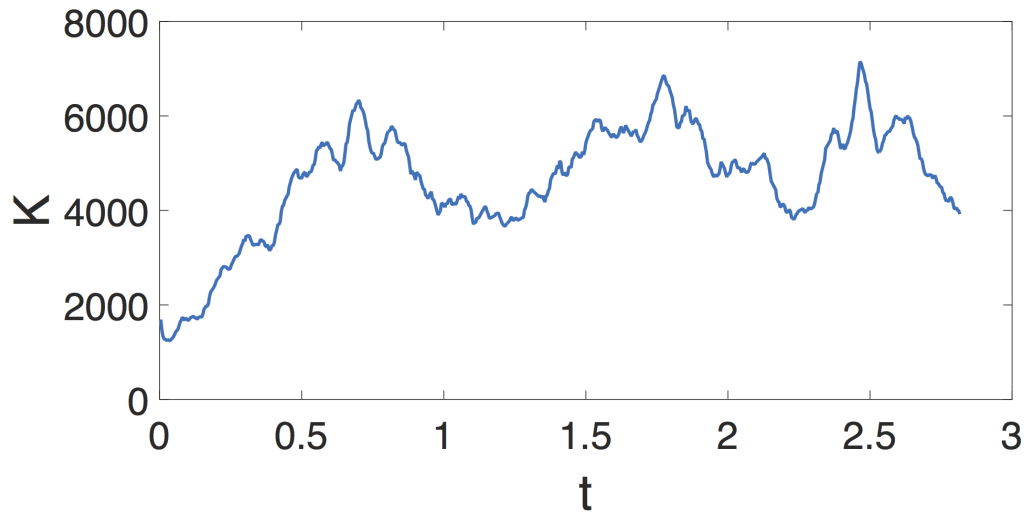


FIG. 6. Number of crossings,  $k$ , as a function of time  $t$  (in s). The average number of crossings for  $t > 0.6$  is  $\bar{k} = 4678.6$

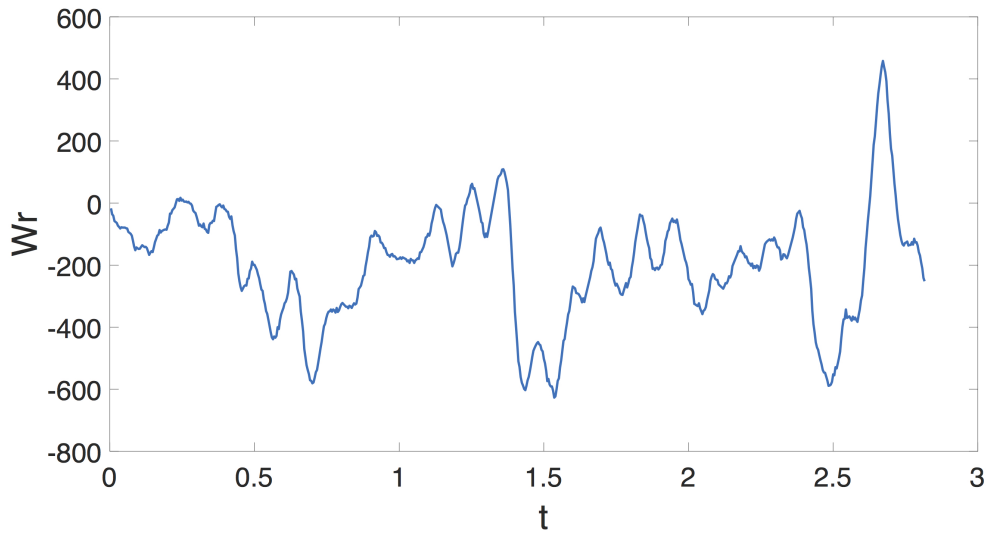


FIG. 7. Writhing number of the vortex tangle,  $Wr$ , as a function of time  $t$  (in s). The average writhing number for  $t > 0.6$  is  $\bar{Wr} = -205.3$ .

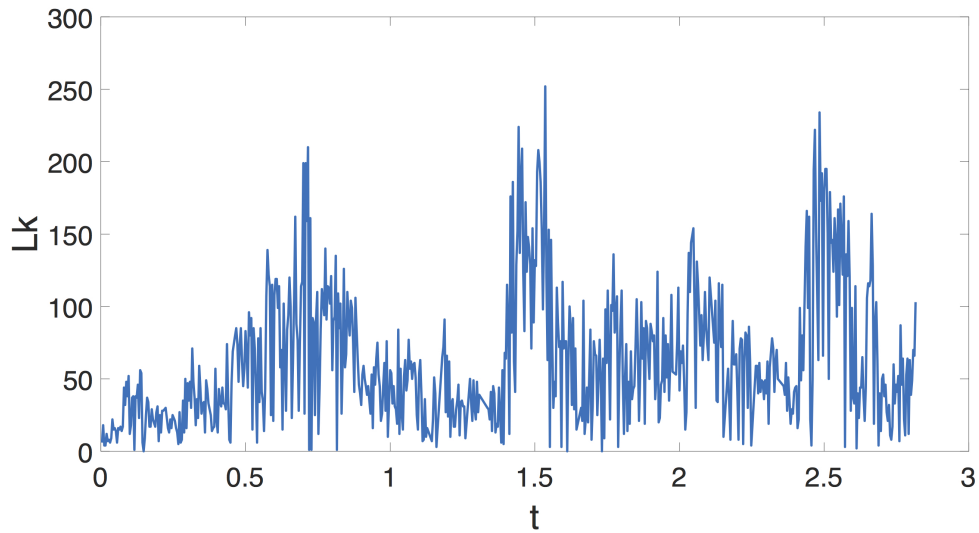


FIG. 8. Total linkage of the tangle,  $Lk$ , as a function of time  $t$  (in s). The average linkage for  $t > 0.6$  is  $\bar{Lk} = 54.0$ .

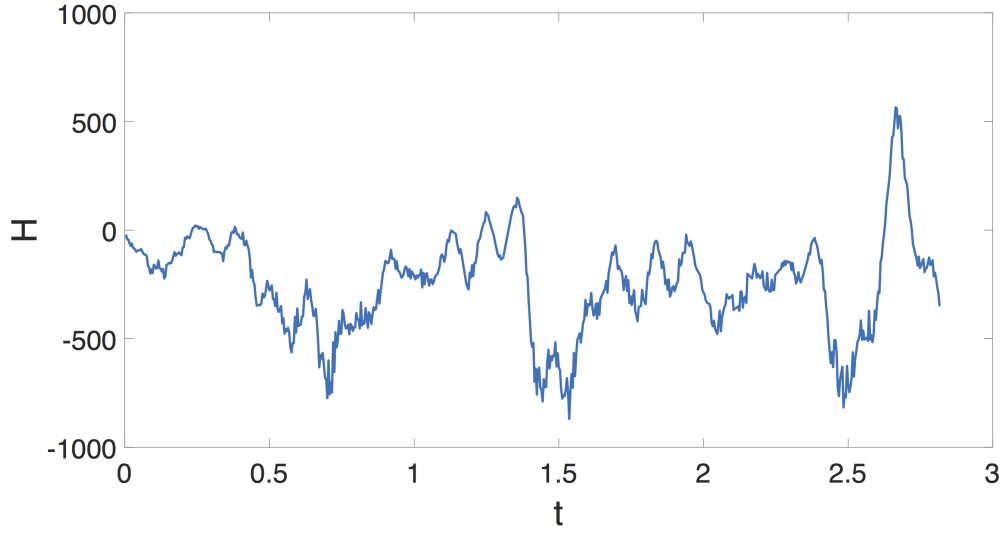


FIG. 9. Centreline helicity of the tangle,  $H$ , (in units of  $\kappa^2$ ) as a function of time  $t$  (in s). The average centreline helicity for  $t > 0.6$  is  $\bar{H} = -325.6$ .

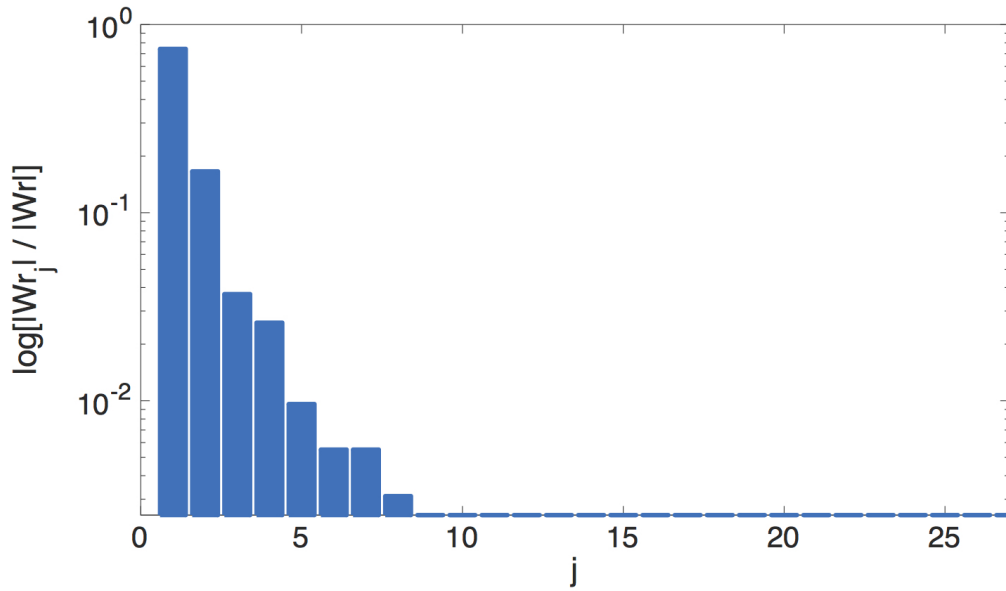


FIG. 10. Relative distribution of writhe,  $\log(|Wr_j|/|Wr|)$ , obtained by averaging over 50 vortex configurations at different times in the saturated regime. At each time, the vortex loop  $j = 1$  has the largest writhe, the loop  $j = 2$  has the second largest writhe, etc. It is apparent that the total writhe of the vortex configuration is due to few large loops.

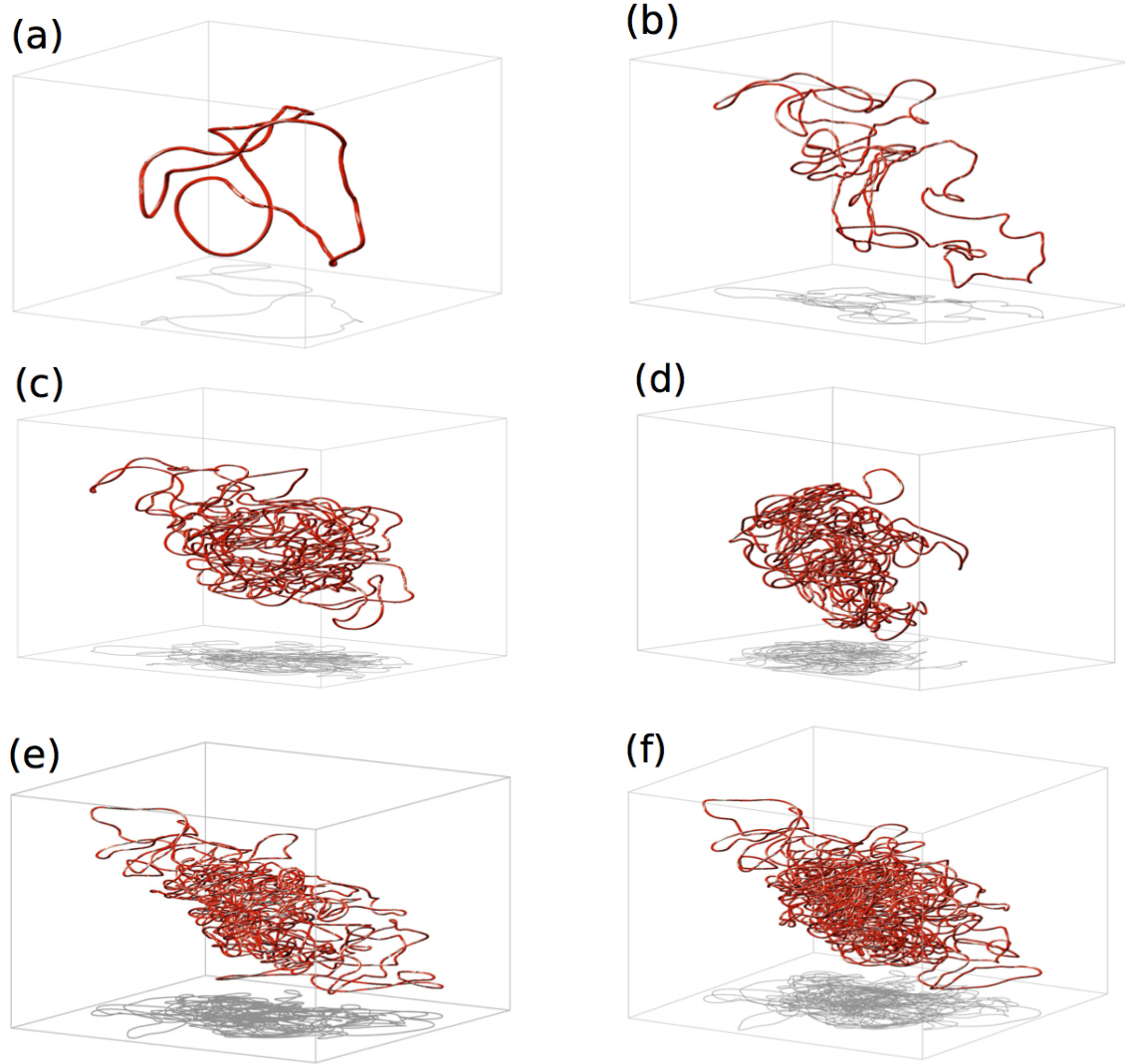


FIG. 11. Examples of vortex loops with given writhing number  $|Wr_j|$ . (a): A vortex loop of 0 writhe. (b): This vortex loop has  $|Wr_j| = 9$ . (c): The writhe of this vortex loop is 21. (d): This loop has a slightly larger writhe of  $|Wr_j| = 92$ . (e): This loop which is the largest at the time has writhe 124. (f): This example is a vortex loop with one of the highest writhes in the whole system with  $|Wr_j| = 124$ .

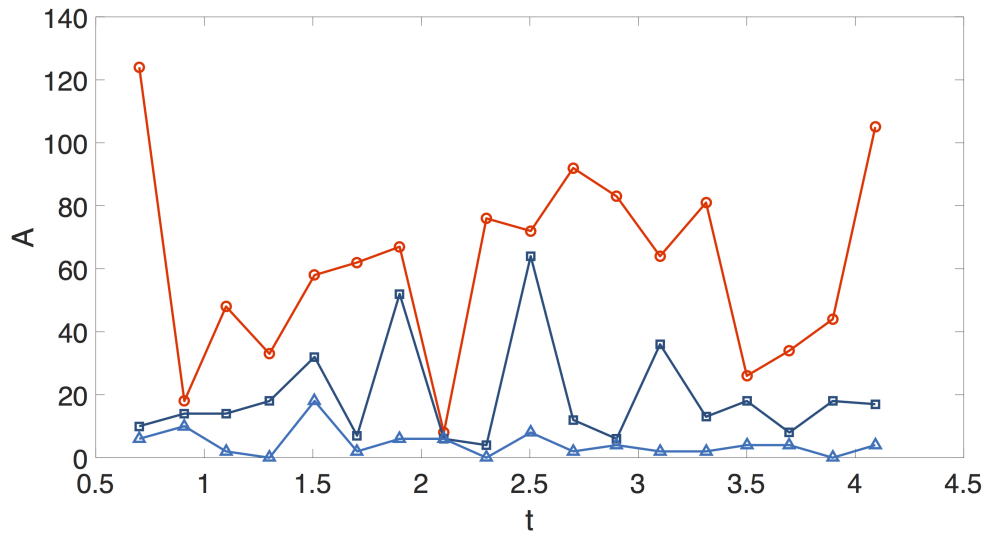


FIG. 12. The evolution of the 1st (red), 2nd (dark blue) and 3rd (light blue) highest orders of Alexander polynomials with time  $t$  (s).

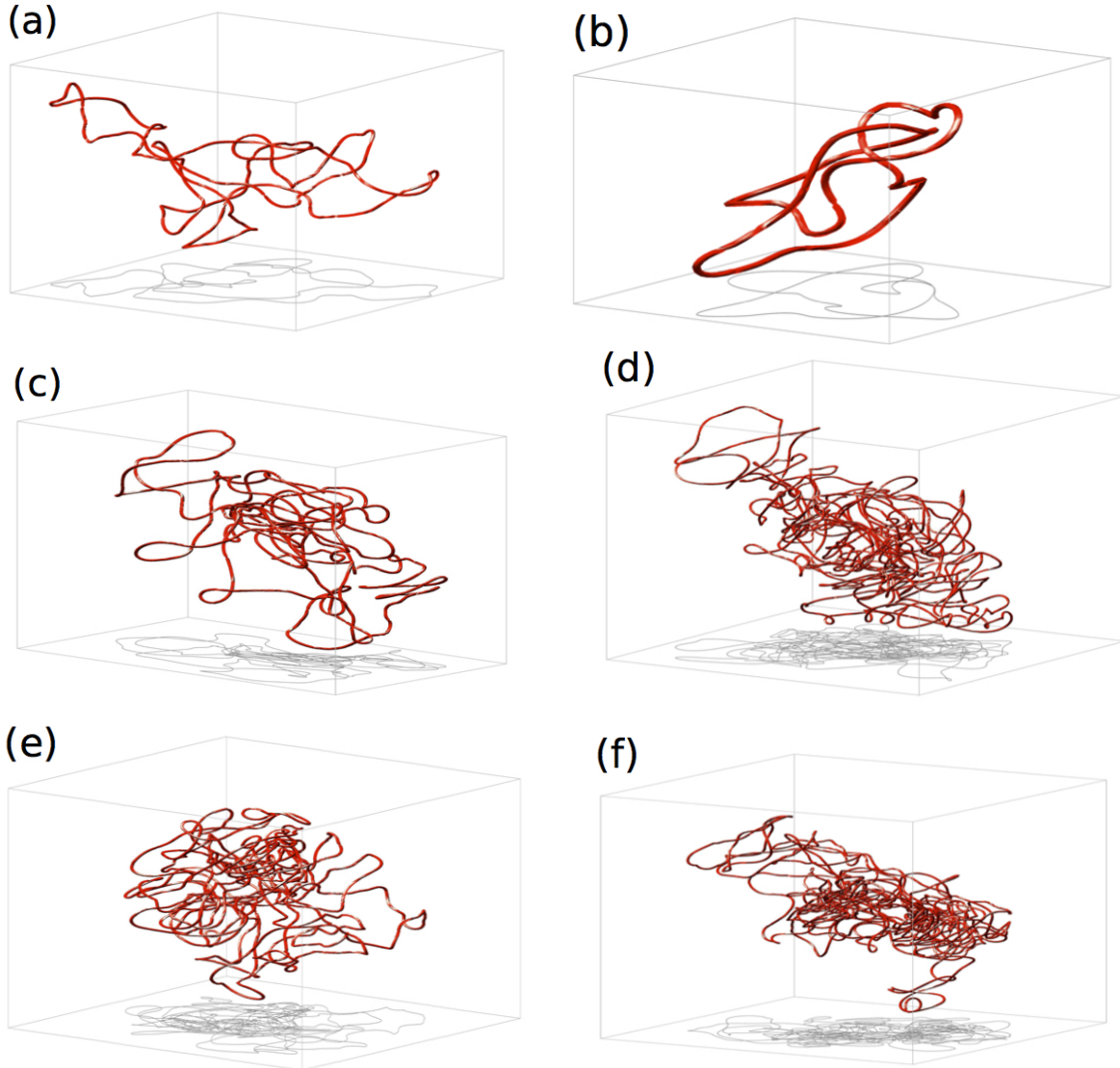


FIG. 13. Examples of vortex loops with given Alexander polynomial of order  $A$  taken from the numerical simulation. (a): A complicated-looking loop which has Alexander polynomial  $\Delta(\tau) = 1$ , so it may be an unknot. (b): This vortex loop has Alexander polynomial  $\Delta(\tau) = 1 - \tau + \tau^2$  which is the polynomial of the trefoil ( $3_1$ ) knot. In fact this particular vortex loop can be easily manipulated into a trefoil by hand. (c): The order of the Alexander polynomial for this loop is 4 as for the Solomon's Seal ( $5_1$ ) knot. (d): This loop has Alexander polynomial of order 18. (e): The Alexander polynomial of this vortex loop is of order 36 (it is not even the highest of the tangle at this particular time). (f): This loop is the largest loop in the tangle at this particular time and has Alexander polynomial of order 83.

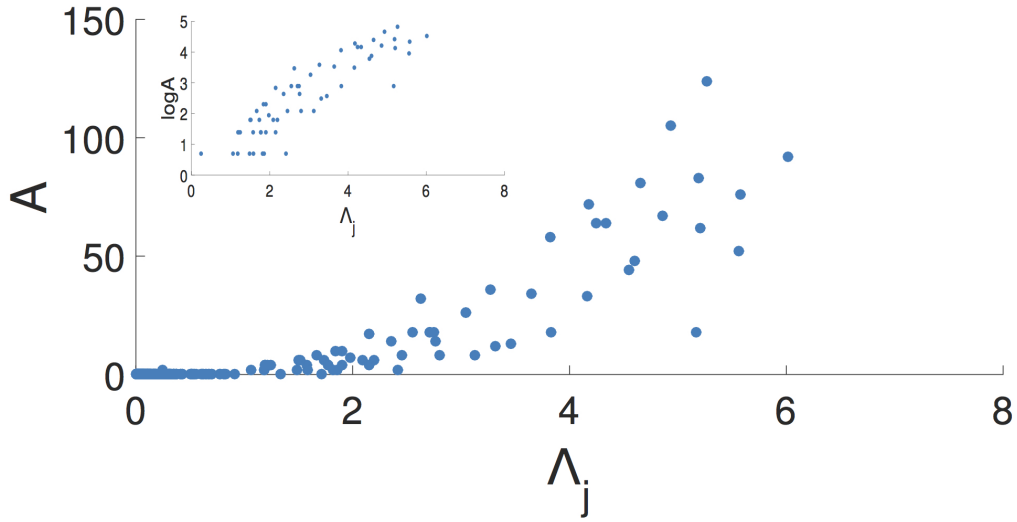


FIG. 14. The relationship between the length of a vortex loop,  $\Lambda_j$  (cm), and the order of its Alexander polynomial,  $A$  (data taken from the time evolution of a single realization).